



RESEARCH ARTICLE

# Effective methylene blue dye removal using groundnut shell-activated nanocarbon

Muppidi Teja Gangadhar Reddy<sup>1</sup>, Prabu Padanillay Chidambaram<sup>1\*</sup>, Jothimani Palanisamy<sup>1</sup>, Jeya Sundara Sharmila Devasahayam<sup>2</sup>, Vijayakumary Ponnaian<sup>3</sup>, Raja Kalimuthu<sup>2</sup> & PM Shanmugam<sup>4</sup>

<sup>1</sup>Department of Environmental Sciences, Tamil Nadu Agricultural University, Coimbatore 641 003, India

<sup>2</sup>Centre for Agricultural Nanotechnology, Tamil Nadu Agricultural University, Coimbatore 641 003, India

<sup>3</sup>Department of Renewable Energy Engineering, Agricultural Engineering College and Research Institute, Tamil Nadu Agricultural University, Coimbatore 641 003, India

<sup>4</sup>Department of Agronomy, Tamil Nadu Agricultural University, Coimbatore 641 003, India

\*Email: [prabu.pc@tnau.ac.in](mailto:prabu.pc@tnau.ac.in)



## ARTICLE HISTORY

Received: 28 September 2024

Accepted: 11 October 2024

Available online

Version 1.0 : 25 December 2024



## Additional information

**Peer review:** Publisher thanks Sectional Editor and the other anonymous reviewers for their contribution to the peer review of this work.

**Reprints & permissions information** is available at [https://horizonepublishing.com/journals/index.php/PST/open\\_access\\_policy](https://horizonepublishing.com/journals/index.php/PST/open_access_policy)

**Publisher's Note:** Horizon e-Publishing Group remains neutral with regard to jurisdictional claims in published maps and institutional affiliations.

**Indexing:** Plant Science Today, published by Horizon e-Publishing Group, is covered by Scopus, Web of Science, BIOSIS Previews, Clarivate Analytics, NAAS, UGC Care, etc See [https://horizonepublishing.com/journals/index.php/PST/indexing\\_abstracting](https://horizonepublishing.com/journals/index.php/PST/indexing_abstracting)

**Copyright:** © The Author(s). This is an open-access article distributed under the terms of the Creative Commons Attribution License, which permits unrestricted use, distribution and reproduction in any medium, provided the original author and source are credited (<https://creativecommons.org/licenses/by/4.0/>)

## CITE THIS ARTICLE

Reddy MTG, Chidambaram PPC, Palanisamy J, Devasahayam JSS, Ponnaian V, Kalimuthu R, Shanmugam PM. Effective methylene blue dye removal using groundnut shell-activated nanocarbon. Plant Science Today.2024;11 (sp4):01-12. <https://doi.org/10.14719/pst.5350>

## Abstract

Activated carbon derived from lignocellulose-rich groundnut shells was synthesized through chemical activation using potassium hydroxide (KOH) to enhance its surface area and porosity. The activation process involved impregnation with KOH and carbonization at elevated temperatures, resulting in groundnut shell-activated nanocarbon (GSANC) with highly developed micro and mesoporous structures. The KOH activation significantly improved the materials' surface area, creating numerous active sites that enhanced its adsorption capacity. This material demonstrated excellent compatibility for removing methylene blue (MB) dye from aqueous solutions, with its adsorption process being driven by electrostatic interactions,  $\pi$ - $\pi$  stacking, and hydrogen bonding. The high affinity of GSANC for MB highlights its potential as an effective adsorbent for wastewater treatment. GSANC exhibited a type I  $N_2$  adsorption-desorption isotherm with an H4 hysteresis loop, indicating a mixture of micro and mesopores, a high specific surface area of 665.802 m<sup>2</sup>/g, and an average pore diameter of 2.97 nm. Its maximum adsorption capacity ( $q_{max}$ ) for MB was 212.766 mg/g.

## Keywords

activated carbon; KOH; groundnut shell; adsorption; methylene blue

## Introduction

Organic dyes impart colour to materials by absorbing light in the visible spectrum. These dyes are categorized based on their chemical structures, including azo dyes, anthraquinone dyes, and phenothiazine dyes (1,2). The synthetic basic dye Methylene Blue (MB) belongs to the phenothiazine group, with the chemical formula C<sub>16</sub>H<sub>18</sub>ClN<sub>3</sub>S (3,4). It is a cationic dye with a positive charge, widely used in industries like textiles, leather, paper, and plastics. It causes significant environmental challenges due to its visibility and toxicity, even at low concentrations (5). Because of its high reactivity and adsorption capability, activated carbon is a highly effective method for removing MB dye from wastewater. However, the cost of activated carbon is a significant drawback. To mitigate this, efforts have been made to produce activated carbon from agricultural wastes containing lignocellulosic compounds, which exhibit properties akin to nanomaterials, offering a more cost-effective and sustainable solution with great potential for removing different pollutants like dyes (6–8). These could be low-cost, eco-friendly,

regenerative, and abundant (9). Groundnut shells are rich in lignocellulosic polymer materials, giving them significant potential as a precursor for biochar and activated carbon production (10).

Activated nanocarbon made from groundnut shells has a high surface area, porous structure, pore diameter, and cation exchange capacity, making it an excellent material for adsorption (11). Even though the activation of biomass can be done by different activation methods physically and chemically, potassium hydroxide KOH is regarded as an effective activator when producing activated carbon with a predominantly microporous structure (12). This study focuses on producing activated carbon from groundnut shells using KOH activation and evaluating its adsorption capacity for removing methylene blue dye from the solution.

## Materials and Methods

Groundnut shells are collected from the Department of Oil Seeds, Tamil Nadu Agricultural University, Coimbatore, India. KOH was procured from Himedia Laboratories Pvt. Ltd., Mumbai, India. Methylene blue was purchased from Isochem Laboratories, Kochi, India.

### Preparation of pristine groundnut shell biochar

Groundnut shells are washed with deionized water and dried in the hot air oven. After drying, shells are pulverized, sieved through a 100-mesh sieve, and stored in a low-moisture environment. Under a limited atmosphere, the crushed shells are pyrolyzed to pristine biochar at 500°C in a pyrolysis unit. After washing with distilled water, the biochar was dried in a hot air oven at 80°C for 24 hours. After pyrolysis, 10 kgs of pulverized groundnut shells yielded 1 kg of biochar. This procedure produced pristine Groundnut Shell Biochar (GSBC).

### Preparation of groundnut shell-activated nanocarbon

GSBC sample of 6.0g was loaded in centrifuge tubes, mixed with 6.0g KOH (1:1 ratio) and 20 distilled water, and oscillated on a shaker for 24 hours. The biochar was dried at 80°C for 24 hours, placed in a ceramic crucible, and activated at 700°C for 2 hours in a muffle furnace with a heating rate of 5°C/min. After cooling, 5g of the modified biochar was mixed with 10 mL of 10% H<sub>2</sub>SO<sub>4</sub> and oscillated for 2 hours to create exfoliated biochar with nanocarbon properties. The product was washed with deionized water and 0.1 mol/L of HCl until neutral pH, then dried at 80°C for 24 hours. The resulting nanocarbon, stored in an inert, low-moisture environment, is called groundnut shell-activated nanocarbon (GSANC).

### Physio-chemical characterization studies

GSBC and GSANC were analyzed for surface morphology using Field Emission Scanning Electron Microscopy (FESEM) with Energy Dispersive Spectroscopy EDS (Tescan - Mira3 XMU, Czech Republic). BET surface area analysis (Quantachrome® ASiQwin™, United States of America) was used for specific surface area measurements. XRD (Shimadzu 6000, Japan) identified mineral composition,

and FTIR (Shimadzu, Japan) detected reactive functional groups. TGA/DTG (EXSTAR/G300) to determine the combustion profile of the materials. Ultimate analysis of raw groundnut shell, groundnut shell biochar, and groundnut shell nano carbon was performed with a CHNS-O analyzer (Thermo Finnigan FLASH EA 1112 Series, United States of America).

### Adsorption studies of MB on GSANC

The adsorption conditions were optimized by varying the GSANC dosage from 0.02 to 0.10g, initial MB concentrations prepared from the stock solution, diluted to 10 to 50 mg/L, and solution pH 2 to 12. 100 mL MB solution in 250 mL Erlenmeyer flasks was stirred in an incubated shaker at 100 strokes/min. Absorbances at 661 nm were measured using a HACH DR 2800 UV-vis spectrophotometer, and concentrations were determined from a calibration curve. The equilibrium isotherm was determined at 303K with initial MB concentrations of 10 to 50 mg/L and contact times of 0 to 360 minutes. The percentage of dye removal (DR%) and adsorption capacity (q<sub>e</sub>) were calculated by (Eqn. 1 and 2), respectively.

$$DR \% = \frac{(C_0 - C_e)}{C_0} \times 100 \quad \dots\dots(Eqn. 1)$$

$$q_e = \frac{(C_0 - C_e)V}{W} \quad \dots\dots(Eqn. 2)$$

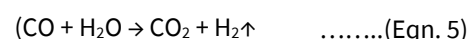
Where; C (mg/L) – Initial concentration of MB dye; C<sub>e</sub> (mg/L) – Equilibrium concentrations of MB dye; q<sub>e</sub> (mg/g) – Amount of dye adsorbed at equilibrium; V (L) – Volume of dye solution; W (g) – GSANC dosage.

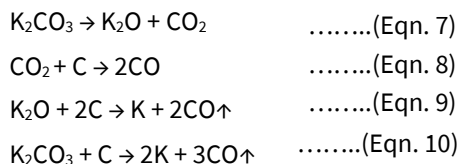
## Results

### Characterization of GSBC and GSANC

#### FESEM with EDS

FESEM micrographs were shown to compare the morphological structures of GSBC (Fig. 1a & 1b) and GSANC (Fig. 1c and 1d). Initially, the biochar surface is uneven but has a smooth texture. After activation with KOH and treatment with 10% H<sub>2</sub>SO<sub>4</sub>, the biochar shows distinct porous features and layered structures, enhancing the formation of micropores and mesopores. This increases the surface-active sites, improving the adsorption capacity for metal ions and organic pollutants. Elemental composition via EDS spectra for GSBC (Fig. 2) and GSANC (Fig. 3) is in (Table 1). KOH is more effective than other chemical agents due to its ability to form intercalation compounds with carbon. The activation process involves carbon gasification, CO<sub>2</sub> release, and the reduction of K<sub>2</sub>O to K, leading to pore development depicted in the (Eqn. 3 to 10) given below (13,14).





framework through redox reactions. Above 700°C, metallic potassium formation (Eqn. 9 and 10) is crucial for developing porosity by incorporating and diffusing potassium into the carbons' internal structure, creating new pores, and expanding existing ones in the final stage.

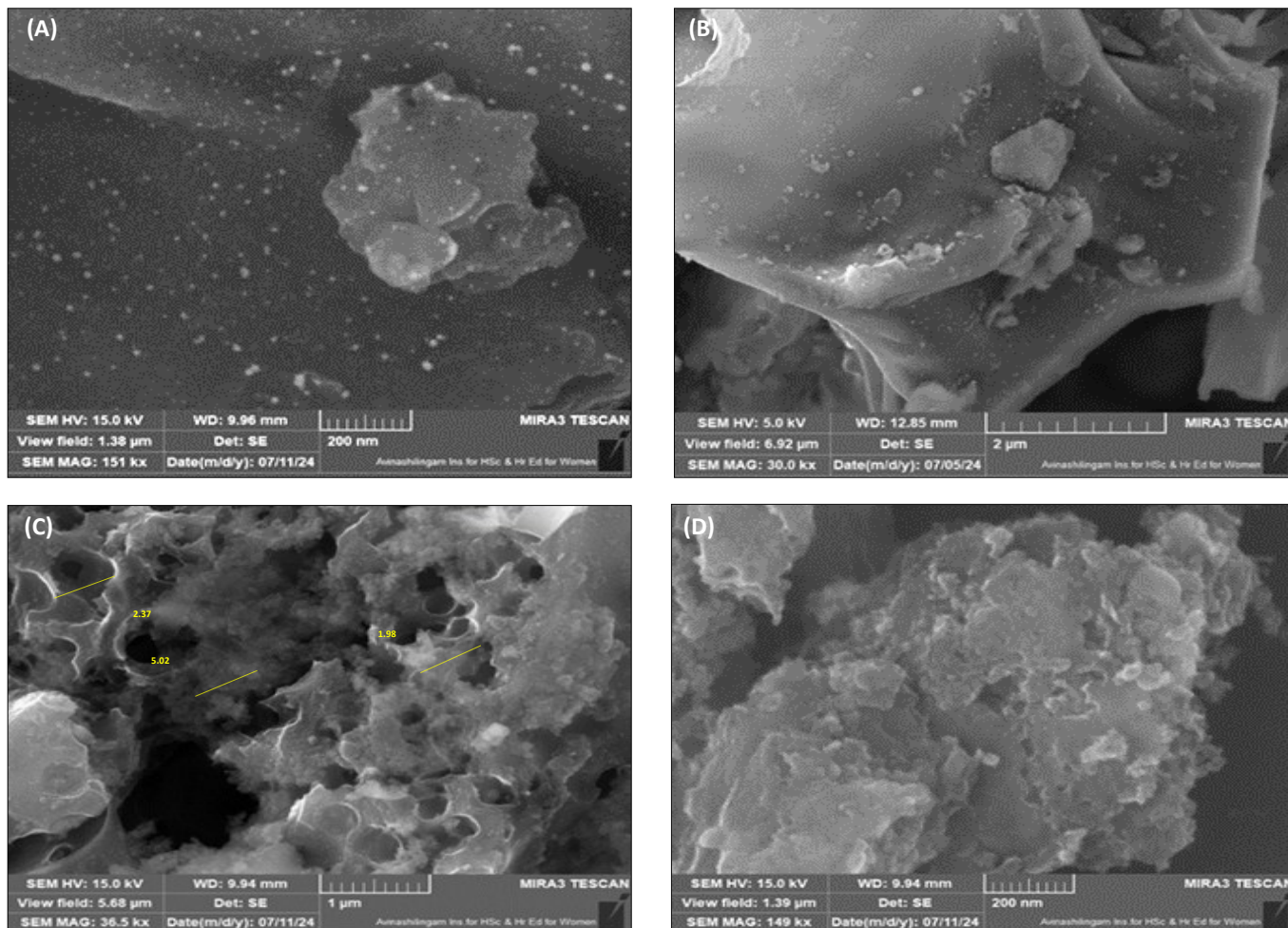


Fig. 1. FESEM micrographs of GSBC (A) 200nm, (B) 2μm, and GSANC (C) 1μm, (D) 200nm.

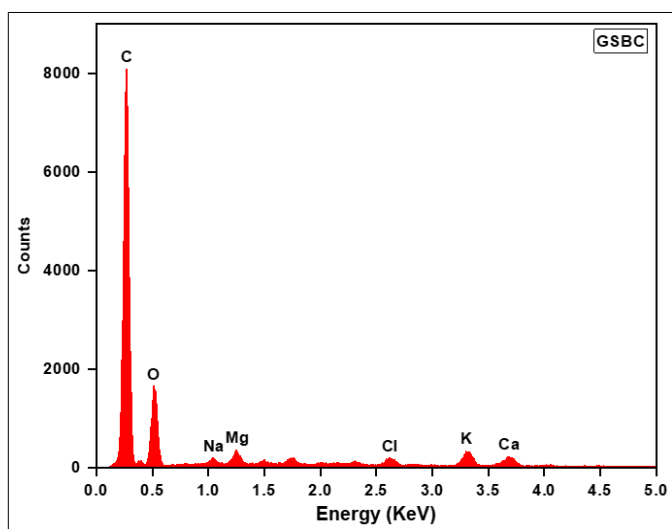


Fig. 2. EDS spectra of GSBC.

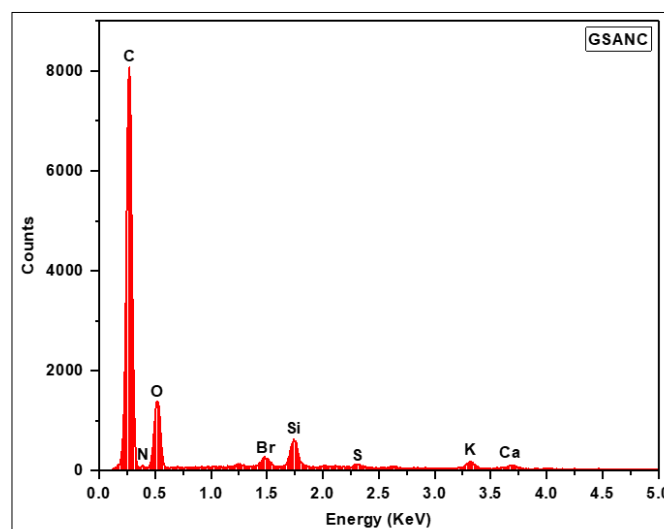


Fig. 3. EDS spectra of GSANC.

The activation of carbon with KOH occurs in three stages.

In the primary stage, H<sub>2</sub>O and CO<sub>2</sub> formation (Eqn. 3 to 5) develop porosity in the carbon. Later, at temperatures near and above 700°C, K<sub>2</sub>O and K<sub>2</sub>CO<sub>3</sub> formation (Eqn. 6 to 8) etches the carbon structure, creating a porous

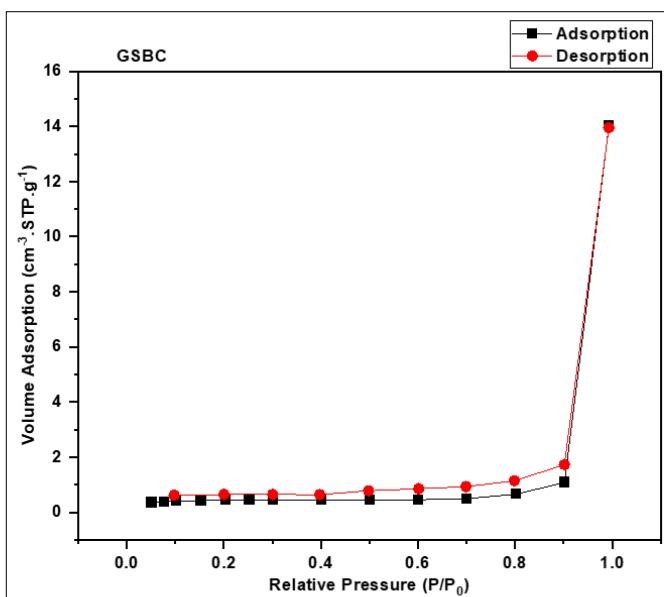
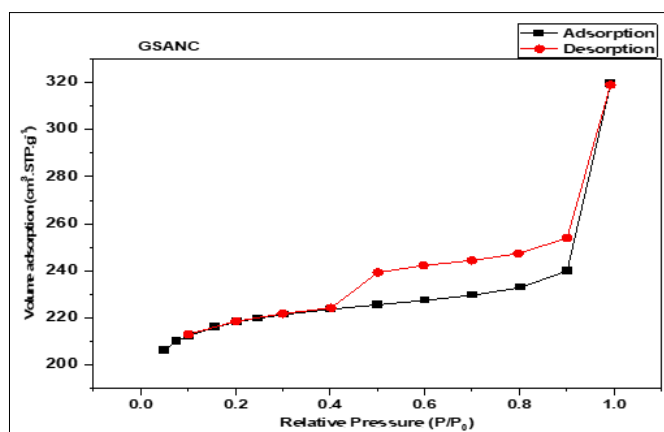
### BET Surface area analysis

Bruneuer-Emmett-Teller surface area analysis shows a substantial rise in the surface area of GSANC compared to GSBC. KOH impregnation at high temperatures increases the surface area and total pore volume by creating porous

**Table 1.** EDS spectral composition of GSBC and GSANC.

Samples		Chemical composition										
		C K	O K	N K	Si K	Br L	K K	Ca K	S K	Cl K	Mg K	Na K
GSBC	Weight %	61.15	27.00	-	-	-	3.83	3.26	-	1.45	1.80	1.51
GSANC	Weight %	66.20	23.93	1.26	3.00	1.77	1.80	1.28	0.77	-	-	-

activated carbon through interactions with gasification. The N<sub>2</sub> adsorption-desorption isotherm plots for GSBC and GSANC are shown in (Fig. 4 and 5) respectively, with textural properties in (Table 2). GSBC shows a rare Type III isotherm, lacking limiting adsorption at high relative pressure (p/p<sub>0</sub>) (Fig. 4). Meanwhile, GSANC shows a Type I isotherm and a Type IV (H4) hysteresis loop (Fig. 5) (15). Similarly, sorghum waste was activated by one mol/L KOH at 800°C for two hours, whereas surface area increased from 0.4 mg/g to 948.6 mg/g in shoot AC and 0.5 mg/g to 168.1 mg/g in root AC (16). Due to micropore filling, GSANC displays a sharp rise in adsorption at low relative pressure. At more significant pressure, however, multilayer adsorption and capillary condensation were observed, signifying the presence of both micropores and mesopores (17). Capillary condensation at p/p<sub>0</sub> above 0.4 suggests broad slit-like mesopores in GSANC. BET analysis reveals that the GSANC has a specific surface area of 665.802 m<sup>2</sup>/g, a total pore volume of 4.95 cc/g, and an average pore diameter of 2.97 nm. Micropores contribute 612.286 m<sup>2</sup>/g (91.96%) of the surface area.

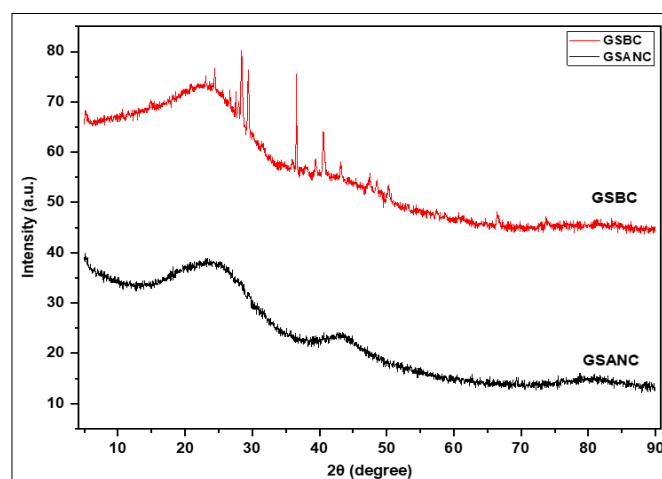
**Fig. 4.** N<sub>2</sub> adsorption-desorption isotherms of GSBC.**Fig. 5.** N<sub>2</sub> adsorption-desorption isotherms of GSANC.**Table 2.** Textural properties of GSBC and GSANC.

Properties	Units	Samples	
		GSBC	GSANC
S <sub>BET</sub>	m <sup>2</sup> /g	1.362	665.802
S <sub>Langmuir</sub>	m <sup>2</sup> /g	0.000	1464.310
S <sub>BJH</sub>	m <sup>2</sup> /g	1.324	103.426
S <sub>Ext</sub>	m <sup>2</sup> /g	0.070	53.516
S <sub>mi</sub>	m <sup>2</sup> /g	1.432	612.286
V <sub>T</sub>	cc/g	2.17	4.95
V <sub>M</sub>	cc/g	0.001	0.316
Average pore size	nm	6.39	2.97
V <sub>BJH</sub>	cc/g	0.021	0.198
W <sub>BJH</sub>	nm	3.623	3.653
Particle size	nm	1034	118

S<sub>BET</sub>: Specific surface area (Brunauer-Emmett-Teller); S<sub>Langmuir</sub>: Specific surface area (Langmuir adsorption isotherm); S<sub>BJH</sub>: Specific Surface Area by Barrett-Joyner-Halenda method; S<sub>Ext</sub>: External Surface Area; S<sub>mi</sub>: Micropore Surface Area; V<sub>T</sub>: Total Pore Volume; V<sub>M</sub>: Micropore Volume; V<sub>BJH</sub>: Pore Volume by Barrett-Joyner-Halenda method; W<sub>BJH</sub>: Pore Width by Barrett-Joyner-Halenda method.

### XRD analysis

The XRD pattern reveals that GSBC exhibits a broad peak near 23° along with distinct sharp peaks at 28.2°, 29°, 37.3°, 40°, and 47° suggesting both crystallinity and the presence of a small quantity of other minerals (11). In contrast, GSANC has distinct peaks at 2θ values of about 23° and 44°, corresponding to the 002 and 100 planes of graphitic crystallites, with broad peaks suggesting an amorphous nature (Fig. 6).

**Fig. 6.** XRD patterns of GSBC and GSANC.

### TGA/DTG analysis

The TGA/DTG analysis of GSBC and GSANC revealed a distinct three-step weight loss (Fig. 7 and 8). The first stage, between 20-200°C, indicated a significant weight reduction corresponding to moisture removal from the sample. The

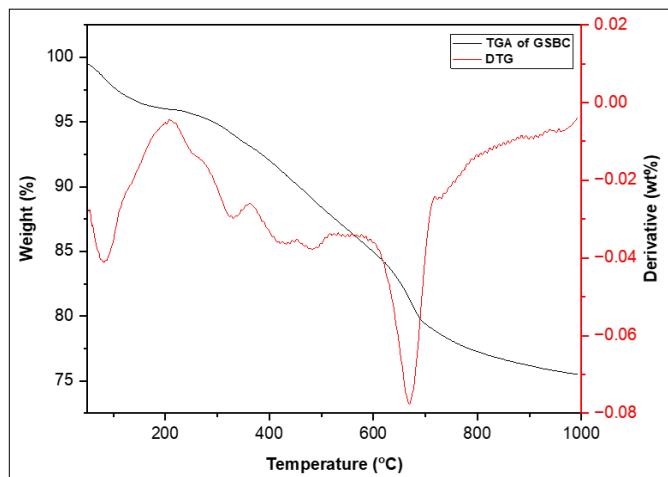


Fig. 7. TGA/DTG results of GSBC.

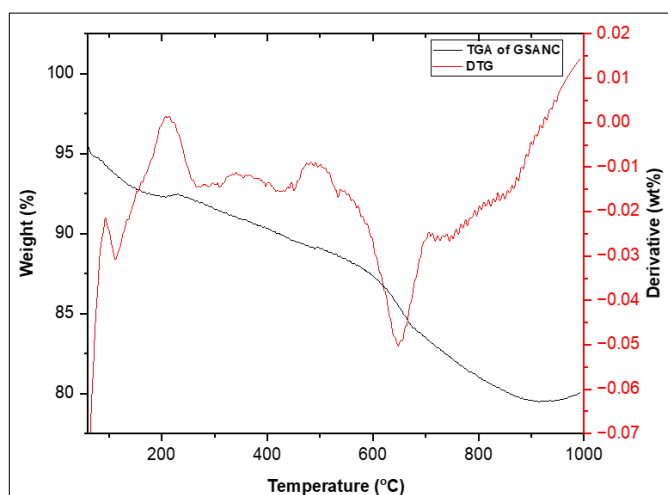


Fig. 8. TGA/DTG results of GSANC.

second stage, between 200-500°C, showed a substantial weight loss attributed to pyrolysis or carbonization, as volatiles and tar substances were eliminated. In the third stage, the breakdown of a high-strength structure was observed during the temperature range of 500-700°C (18). Beyond 700°C, the weight loss was minimal, indicating the stability of the adsorbents' basic structure.

### FT-IR analysis

FT-IR (Fourier Transform Infrared) analysis is widely used to identify the functional groups on the surface of activated carbon and provides valuable insight into the chemical composition of GSANC. Functional groups such as carboxyl (-COOH) and hydroxyl (-OH) are particularly beneficial, as they can interact with positively charged dye molecules. A more significant number of these desirable functional groups on the surface of activated carbon enhances its adsorption capacity, especially for cationic dyes like methylene blue (19). The functional groups detected by FT-IR analysis shows for GSBC (Fig. 9), absorption at 1553.488  $\text{cm}^{-1}$  (N-O stretching), 1397.537  $\text{cm}^{-1}$  (C-O stretching), 689.192  $\text{cm}^{-1}$  (C=C bending), and 511.901  $\text{cm}^{-1}$  (C-Cl stretching). For GSANC, absorption at 3819.699  $\text{cm}^{-1}$  (OH stretch), 3628.454  $\text{cm}^{-1}$  (alcoholic OH stretch), 3090.834  $\text{cm}^{-1}$  (=C-H stretch), 2326.675  $\text{cm}^{-1}$  (C=N nitrile stretch), 1505.882  $\text{cm}^{-1}$  (C=O amide stretch), and 713.816  $\text{cm}^{-1}$  (C=C bending) as shown in Fig. 10.

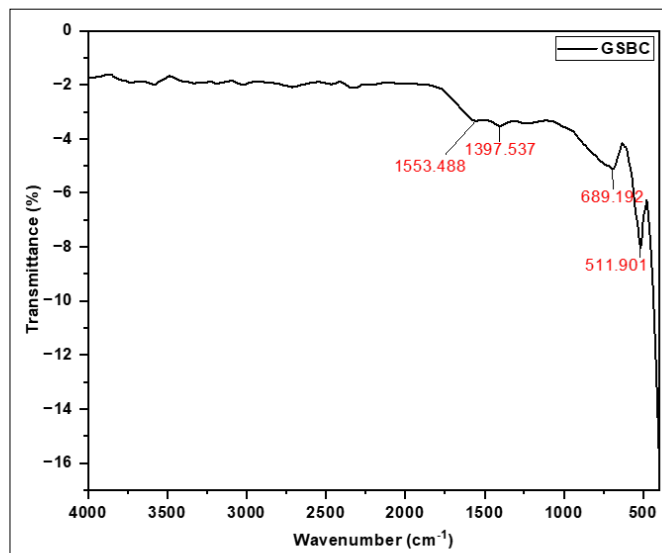


Fig. 9. FT-IR spectra of GSBC.

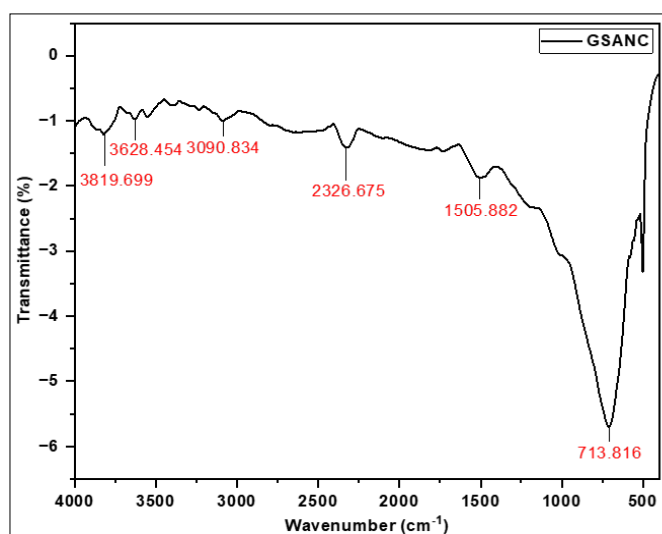


Fig. 10. FT-IR spectra of GSANC.

### Ultimate analysis

From the Ultimate analysis, the H/C molar ratio indicator of the degree of aromaticity and stability of GSBC and GSANC was calculated at 0.02 and 0.05, respectively, falling below the threshold of 0.7, aligning with the standards set by the IBI (20) and EU guidelines (21). Similarly, the O/C molar ratio indicates the oxidation level and the extent of carbonization of GSBC and GSANC was 0.18 and 0.208, meeting the EU guidelines' requirement of being below 0.4.

### Adsorption Studies

#### Effect of GSANC dosage

The effect of GSANC dosage on the removal of MB dye was investigated by varying the adsorbent amount from 0.02 to 0.10 grams while maintaining all other parameters as constant, as shown in (Fig. 11). The efficiency of MB dye removal increased significantly from 24.2 to 99.9 % as the adsorbent dosage was increased 0.02 to 0.08 grams. It was clear that increasing the adsorbent dose to more than 0.08 grams cannot show any significant dye removal. Since the maximum removal of MB dye ions of 99.9 % was achieved with a 0.08 gram dosage, this amount of GSANC was selected for future applications.

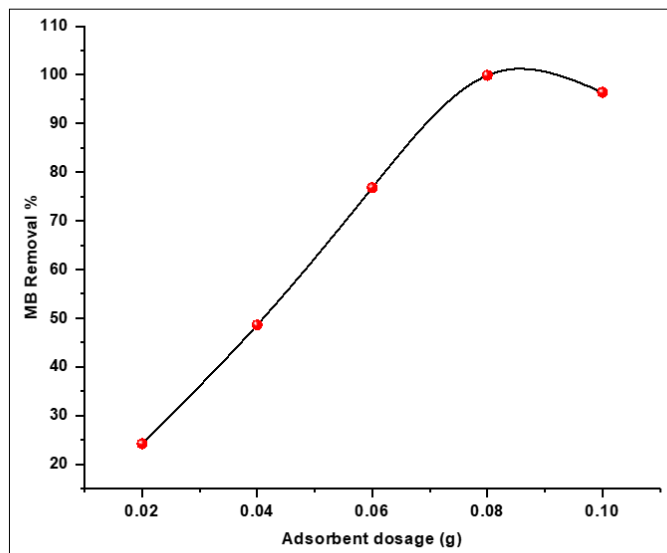


Fig. 11. Effect of adsorbent dosage on MB removal %.

### Influence of pH

The pH of a solution significantly affects the adsorption process by modifying the adsorbents' surface charge and the adsorbate molecules' ionization degree. To investigate the effect of pH on the removal of MB dye ions, experiments were carried out across a pH range of 2-12 using an optimized dosage of GSANC while keeping other parameters constant (30 mg/L concentration, 0.08 grams adsorbent dosage, 360 minutes contact time). Understanding MB dye uptake at various pH levels requires identifying where the adsorbent's surface has a neutral net charge, known as the point of zero charge (pH<sub>zpc</sub>). The pK<sub>a</sub> value of MB dye, which is 3.8, indicates that MB dye molecules exist in cationic form in the solution. The pH<sub>zpc</sub> of GSANC is slightly basic at 7.2. The highest adsorption capacity of 45.35 mg/g was observed at pH 8 (Fig. 12), a fundamental condition where the GSANC surface acquires a negative charge, attracting MB molecules through electrostatic attraction. At the lowest pH values of the adsorbent, repulsive electrostatic attraction is forced between MB dye ions and positively charged functional groups of GSANC adsorbent. At the alkaline pH of the solution, the adsorbent becomes negatively charged, leading to the effective removal

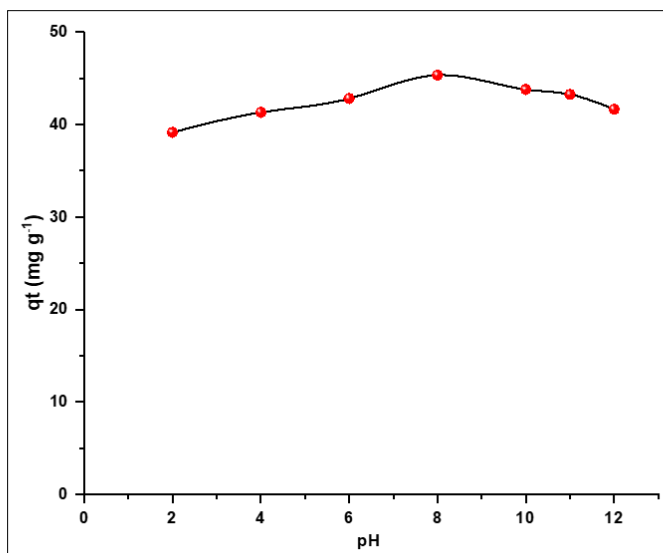


Fig. 12. Effect of pH on adsorption capacity.

of cationic MB dye ions. Consequently, pH 8 is the optimized pH solution for further experiments.

### Effect of the initial concentration and contact time

The effects of contact time and initial concentrations of MB dye (ranging from 10 to 50 mg/L) on the adsorption capacity of GSANC were evaluated using optimized parameters. The adsorption capacities of GSANC at a specific time, denoted as  $q_t$  (mg/g), were plotted against time (min) for various MB dye concentrations, as illustrated in (Fig. 13). The adsorption capacity of GSANC was observed to increase by 12.48 to 45.35 mg/g as the concentration of MB dye rose 10 to 50 mg/L. In the early stages of the process, there was a swift increase in adsorption capacity at all concentrations, likely due to the abundance of available adsorption sites on the GSANC for MB dye uptake. As the process progressed, the adsorption rate gradually declined and eventually stabilized, signaling that equilibrium between the adsorbent and the adsorbate was being reached. Equilibrium times for the GSANC-MB interaction were achieved at 210, 270, 300, 330, and 330 minutes for concentrations of 10, 20, 30, 40, and 50 mg/L, respectively. At higher MB dye concentrations, more time was needed to achieve equilibrium due to the concentration gradient, which facilitates the diffusion of dye into the internal pores and surface of the adsorbent.

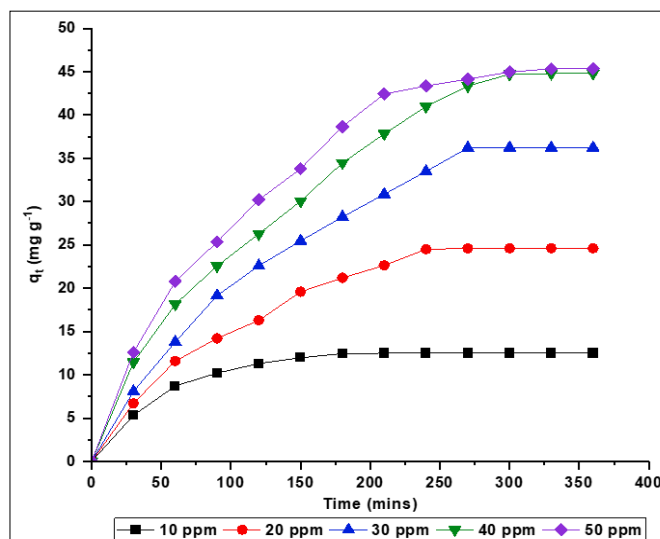


Fig. 13. Effect of the contact time on MB dye adsorption on GSANC at different initial concentrations.

### Adsorption kinetics and modelling

Understanding the kinetics and identifying the rate-determining step is essential to design an effective adsorption system. In this study, three kinetic models' pseudo-first-order (PFO) (22), pseudo-second-order (PSO) (23), and Elovich (24) were applied to the experimental data to elucidate the adsorption mechanism of MB dye on GSANC. Linear forms of these models were used to minimize statistical bias. The best-fitted model was selected based on the highest coefficient of determination ( $R^2$ ) from the respective equations for PFO (Eqn. 11), PSO (Eqn. 12), and Elovich (Eqn. 13a and 13b).

$$\log(q_e - q_t) = \log q_e - \frac{k_1}{2.303} t \quad \dots\dots(\text{Eqn. 11})$$

$$\frac{t}{q_1} = \frac{1}{k_2 q_e^2} + \frac{t}{q_e} \quad \dots\dots(\text{Eqn. 12})$$

$$\frac{dq_t}{dt} = \alpha e - \beta q_t \quad \dots\dots(\text{Eqn. 13a})$$

$$q_t = q_o + \frac{1}{\beta} \ln(\alpha\beta) + \frac{1}{\beta} \ln(t) \quad \dots\dots(\text{Eqn. 13b})$$

Where;  $k_1$  (per min) – Lagergren's PFO kinetic parameter;  $q_t$  (mg/g) – Amount of dye adsorbed at time  $t$ ;  $q_e$  (mg/g) – Amount of dye adsorbed at equilibrium;  $k_2$  (mg/g/min) – PSO kinetic parameter;  $\alpha$  (mg/g/min) – Initial adsorption rate;  $\beta$  (g/mg) – Extent of surface coverage and the activation energy for chemisorption.

Using an initial concentration ( $C_o$ ) of 30 mg/L, (Fig. 14,15,16) illustrates the PFO, PSO, and Elovich model plots, while (Table 4) presents the extracted parameters and their  $R^2$  values. The analysis shows that MB adsorption by GSANC follows the PSO model, as indicated by higher  $R^2$  values.

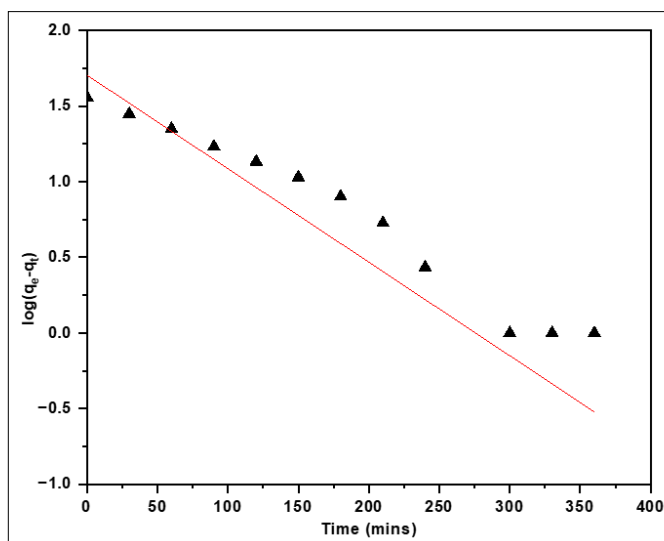


Fig. 14. PFO model for MB dye adsorption by GSANC.

### Isotherm modelling

The adsorption capacities of GSANC were evaluated at initial concentrations of 30, 40, and 50 mg/L. The interac-

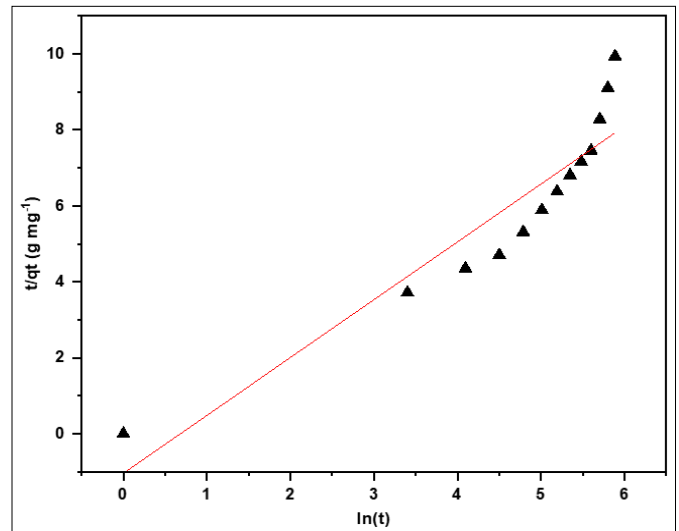


Fig. 15. PSO model for MB dye adsorption by GSANC.

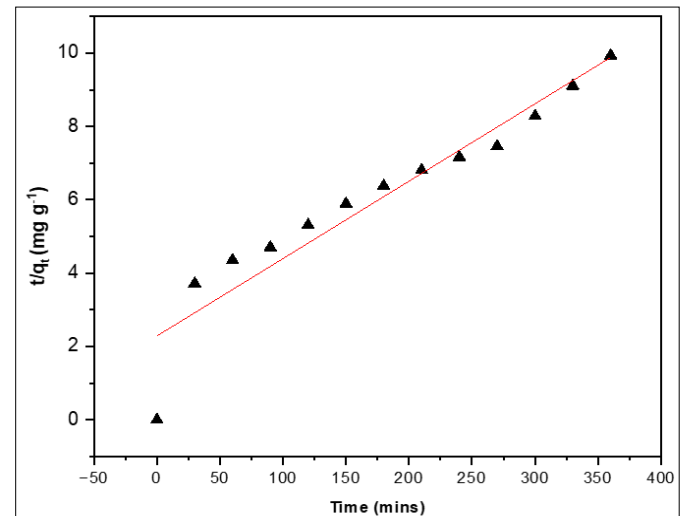


Fig. 16. Elovich model for MB dye adsorption by GSANC.

tion between MB dye and GSANC was analyzed using Langmuir and Temkin isotherm models (25, 26, 27). The Langmuir model describes monolayer adsorption on fixed sites (Eqn. 14a), with the Langmuir constant  $R_L$  given in (Eqn. 14b). The Freundlich model describes multilayer adsorption on heterogeneous surfaces (Eqn. 15). The Temkin model accounts for a decrease in adsorption heat with increased coverage, reflecting adsorbent-adsorbate interactions (Eqn. 16).

$$\frac{C_e}{q_e} = \frac{1}{K_L X_m} + \frac{C_e}{X_m} \quad \dots\dots(\text{Eqn. 14a})$$

$$R_L = \frac{1}{1 + K_L C_o} \quad \dots\dots(\text{Eqn. 14b})$$

Table 4. Pseudo First Order (PFO), Pseudo Second Order (PSO) and Elovich kinetic parameters for MB dye adsorption by GSANC.

$C_o$ (mg/L)	PFO			PSO			Elovich		
	$q_e$ cal (mg/g)	$k_1$ (mg/g/min)	$R^2$	$q_e$ cal (mg/g)	$k_2$ (mg/g/min)	$R^2$	$\alpha$	$\beta$	$R^2$
10	4.45	0.004	0.43	13.47	0.003	0.99	1.86	0.42	0.95
20	5.23	0.005	0.56	30.21	0.0004	0.94	2.02	0.21	0.87
30	6.01	0.006	0.53	47.39	0.0001	0.90	2.46	0.14	0.83
40	7.17	0.006	0.56	57.14	0.0001	0.90	3.09	-2.1	0.84
50	8.05	0.006	0.51	58.24	0.0002	0.94	3.65	-2.1	0.87

$C_o$ : initial concentration;  $q_e$ : Amount of dye adsorbed at equilibrium;  $k_1$ : Lagergren's PFO kinetic parameter;  $R^2$ : coefficient of determination;  $k_2$ : PSO kinetic parameter;  $\alpha$ : Initial adsorption rate;  $\beta$ : Extent of surface coverage and the activation energy for chemisorption.

$$\log q_e = \log k_f + \frac{1}{n} \log c_e \dots\dots(Eqn. 15)$$

$$q_e = \frac{RT}{B} \ln K_T + \frac{RT}{B} \ln C_e \dots\dots(Eqn. 16)$$

Where;  $q_e$  (mg/g) – Amount of dye adsorbed at equilibrium;  $C_e$  (mg/L) – Equilibrium dye concentration;  $X_m$  (mg/g) – Maximum adsorption capacity;  $K_L$  – Langmuir constant;  $C_0$  – Initial concentration;  $k_f$  and  $n$  – Freundlich constants;  $B$  (J/mol) – Temkin constant;  $k_T$  (L/g) – Temkin isotherm energy constant;  $b_T$  (J/mol) – Heat of adsorption;  $R$  – Gas constant (8.314 J/mol K).

Based on  $R^2$  values from the isotherm models in (Table 5), the adsorption of MB onto the GSANC surface was analyzed. The Langmuir, Freundlich, and Temkin isotherms for MB dye adsorption by GSANC, with a constant adsorbent dosage of 0.08 grams, solution pH of 8, temperature set at 30°C (303 K), an agitation speed of 150 strokes, and a 100 mL volume of MB solution are illustrated in (Fig. 17 to 19). The adsorption of MB on the GSANC surface followed the Langmuir adsorption isotherm, indicating that the MB uptake occurred as a monolayer on homogeneous, fixed adsorption sites. The  $q_{max}$  value of 212.766 mg/g at 30°C demonstrates the adsorption capacity of MB dye ions on GSANC at elevated temperatures.

**Adsorption thermodynamics**

The thermodynamic parameters, including Gibbs free energy ( $\Delta G^\circ$ ), enthalpy ( $\Delta H^\circ$ ), and entropy ( $\Delta S^\circ$ ), for the adsorption of methylene blue (MB) dye ions onto GSANC, were determined at varying temperatures (30°C, 40°C, 50°C, and 60°C), as described by Eqns. 17, 17a, 19, and 20.

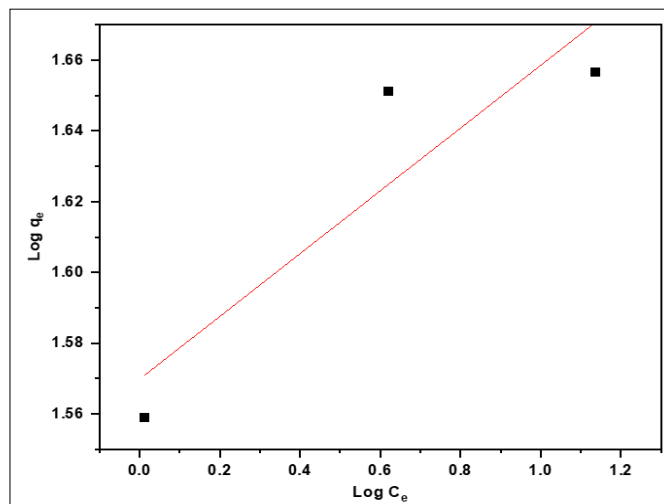


Fig. 18. Freundlich adsorption isotherm of MB dye adsorption by GSANC.

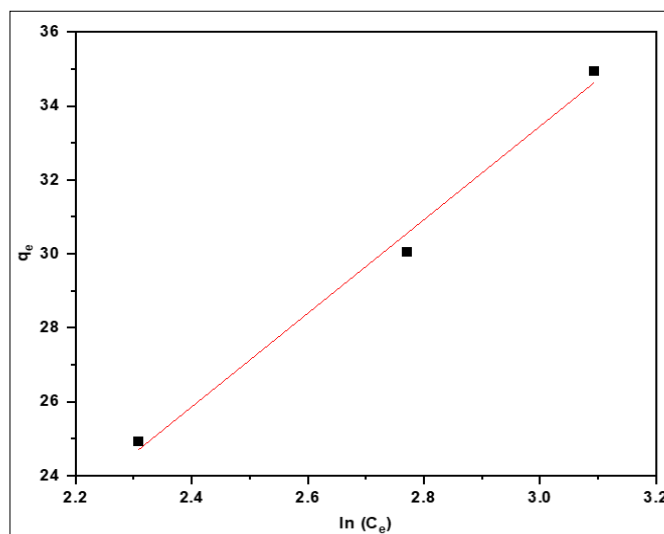


Fig. 19. Temkin adsorption isotherm of MB dye adsorption by GSANC.

Table 5. Parameters of isotherm models for MB dye adsorption by GSANC at 30°C.

Adsorption isotherm	Langmuir			Freundlich			Temkin		
Parameter	$q_{max}$ (mg/g)	$K_L$	$R^2$	$K_f$ (mg/g) (L/mg) <sup>1/n</sup>	$n$	$R^2$	$K_T$ (L/mg)	$b_T$ (J/mol)	$R^2$
Value	212.766	0.21659	0.9999	1.2268	0.6370	0.8277	0.6995	199.00	0.992

$q_{max}$ : Maximum adsorption capacity;  $K_L$ : Langmuir constant;  $R^2$ : coefficient of determination;  $K_f$  &  $n$ : Freundlich constants;  $K_T$ : Temkin isotherm energy constant;  $b_T$ : Heat of adsorption.

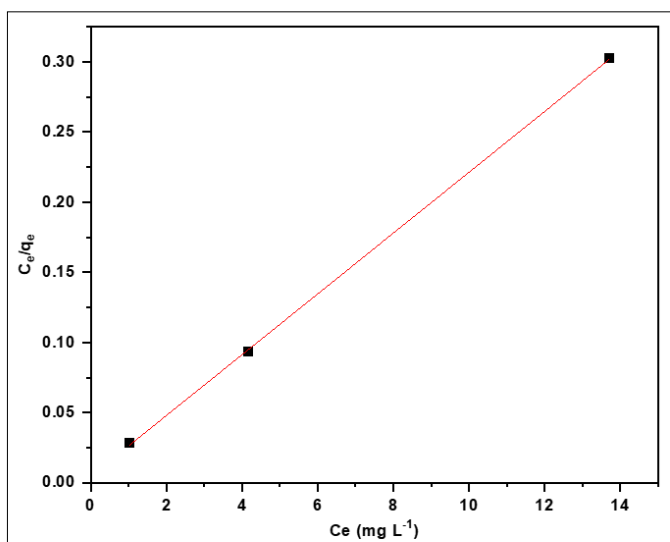


Fig. 17. Langmuir adsorption isotherm of MB dye adsorption by GSANC.

$$\Delta G = - RT \ln K \dots\dots(Eqn. 17)$$

Whereas,  $K = \frac{q_e}{C_e (Q_0 - q_e)}$  .....(Eqn. 17a)

Vant Hoffs' equation:  $\ln K_d = \frac{\Delta S^\circ}{R} - \frac{\Delta H^\circ}{RT}$  .....(Eqn. 18)

By vant hoffs' plot (28) (Eqn. 18) of  $\ln K$  versus  $\frac{1}{T}$  thermodynamic parameters was determined, as shown in Fig. 20. determination of  $\Delta H$  and  $\Delta S$  from the slope and intercept has been done, respectively (Table 6).

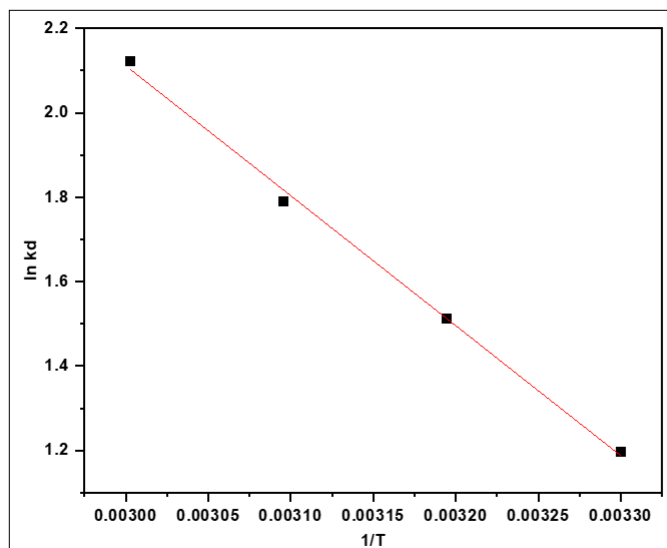


Fig. 20. Vant Hoffs' plot (GSANC adsorption of MB dye).

Table 6. Thermodynamic parameters for the adsorption of MB dye on GSANC.

Temp (°C)	Temp (K)	$K_d$	$\Delta G$ (KJ/mol)	$\Delta H$ (KJ/mol)	$\Delta S$ (KJ/mol)
30	303	3.305394	-2.98915		
40	313	4.531684	-3.93229	25.588	0.094314
50	323	5.983796	-4.87543		
60	333	8.33589	-5.81857		

$K_d$ : Distribution coefficient;  $\Delta G$ : Gibbs energy;  $\Delta H$ : Enthalpy;  $\Delta S$ : Entropy.

$$\text{Slope} = \frac{\Delta H^\circ}{R} \therefore \Delta H^\circ = -(\text{Slope} \times R) \quad \dots\dots\dots(\text{Eqn. 19})$$

$$\text{Intercept} = \frac{\Delta S^\circ}{R} \therefore \Delta S^\circ = \text{Intercept} \times R \quad \dots\dots\dots(\text{Eqn. 20})$$

Where;  $K_d$  – Distribution coefficient;  $\Delta G$  – Gibbs energy;  $\Delta H$  – Ethalpy;  $\Delta S^\circ$  – Entropy.

The thermodynamic parameters show that the distribution coefficient ( $K_d$ ) increases with temperature, indicating improved adsorption capacity of GSANC for Methylene Blue (MB) dye. Negative  $\Delta G$  values signify that the adsorption process is spontaneous, whereas positive  $\Delta H^\circ$  values indicate that the process is endothermic. Positive  $\Delta S^\circ$  values suggest that MB dye displaces water molecules on GSANC. The increasing  $K_d$  values with increasing temperature further highlight the endothermic nature of the adsorption process, showing that higher temperatures improve the adsorption of MB dye ions by GSANC. The experiment was conducted at room temperature, approximately 30°C, which was identified as the optimal temperature. This temperature recorded The maximum adsorption capacity at 212.766 mg/g.

## Discussion

GSANC offers exceptional properties that make it highly effective for methylene blue (MB) adsorption in wastewater treatment due to its enhanced surface area, porous structure, and stability. The high adsorption capacity of GSANC stems from its well-developed structural

characteristics such as surface area, porosity, pore diameter, amorphous nature of the material and its stability. The groundnut shell activated with KOH exhibited similar well-developed properties, achieving a maximum methylene blue adsorption capacity of 332.20 mg/g (29). Similarly, a maximum adsorption capacity of 208 mg/g for activated carbon was derived from groundnut shells, highlighting its exceptional properties for effective adsorption (30).

## Characterization studies of GSBC and GSANC

In our study, FESEM micrographs show that the GSANC contains a more porous structure than GSBC. The average pore size was recorded as 2.97 nm, and a layered structure was formed due to the exfoliation process. Recent studies related to the surface area of ACs have recorded that the formation of voids on the surface is due to the evaporation of potassium hydroxide during activation, creating cavities previously filled by the potassium hydroxide (16,30). Rape-seed biochar activated at 450°C exhibited a pore size of 1.2 nm, while activation at 700°C resulted in a pore size of 1.6 nm. In comparison, groundnut shell-activated carbon (GSANC) demonstrated a larger pore size, enhancing its potential for greater adsorption capacity (31). EDS spectra state a more than 5 % increase in the weight % of carbon and a slight decrease in the oxygen weight %. There was a high rise in carbon content (86.88 wt%) in the KOH-activated groundnut shells, whereas low carbon content (31.02 wt%) was reported in the AC produced from  $H_3PO_4$  (29).

The appearance of a Type I isotherm combined with a Type IV (H4) hysteresis loop in the  $N_2$  adsorption-desorption analysis of GSANC indicates that most of its porosity is within the micropore range. This aligns with the development of microporous channels formed during the activation process of the carbon material (32) and exhibits 665.802  $m^2/g$  with a micropore contribution of 612.286  $m^2/g$  (91.96%), a total pore volume of 4.95 cc/g, and an average pore diameter of 2.97 nm. The impregnation ratio of KOH and biochar and activation temperature affect the pore volume, structure, pore diameter and surface area of activated carbon. Recent findings by (33) made AC by impregnating KOH to pre-carbonized groundnut shells at 650°C increased specific surface area from 3.5 to 363.1  $m^2/g$ . Activated carbon made from groundnut shell with KOH (1:1 ratio) at 600°C had a recorded surface area of 412  $m^2/g$  and MB removal value of 83.33 mg/g, potentially helpful for wastewater treatment (34). KOH-activated carbon yielded the highest BET surface area at 691.69  $m^2/g$ , outperforming other activating agents like  $H_3PO_4$  and  $ZnCl_2$ . The high surface area will give the contaminants contaminants a high advisor.

In XRD patterns, carbon crystallites are generally classified into A sharp and narrow reflection pattern, which indicates graphitized carbon, like GSBC. In contrast, a broad reflection pattern indicates non-graphitized carbon, depicted as GSANC. In GSBC, the XRD pattern reveals that it exhibits several distinct sharp peaks at 28.2°, 29°, 37.3°, 40°, and 47°, suggesting both crystallinity and the presence of a small number of other minerals. Similar results have been reported in a recent study by (35), where

KOH-activated groundnut shell carbon exhibits a crystalline carbonaceous structure, as indicated by a curve with three characteristic sharp peaks at angles of 25°, 30°, 38°, 40°, and 50°. The XRD pattern of GSANC reveals that the broad peaks at 23° and 44° depict the amorphous nature of the AC. The peak at around 44° (100 plane) is from honeycomb structures formed by sp<sup>2</sup> hybridized carbon framework (36). The amorphous nature of porous activated carbon was prepared, which exhibited peaks around 24° and 43.4° corresponding to 002 and 100 planes, respectively, exhibiting the amorphous nature (37). In TGA/DTG analysis, substantial weight loss was observed between 200 and 500°C. It represents the high weight loss observed in both GSBC and GSANC. Above the temperature of 500°C, loss in weight was minuscule, demonstrating that the basic structure of the char was formed and became almost constant. A residual trace of celluloses and hemicelluloses was obtained. The significant fraction comprises lignin, as it is difficult to break down. Studies have revealed that lignin decomposition happens slowly from 200 to 900°C (11,38,39). FT-IR analysis states that GSANC has absorption at 3819.699 cm<sup>-1</sup> (water -OH stretch) and 3628.454 cm<sup>-1</sup> (alcoholic -OH stretch) functional groups are present at the 3200 to 3900 per cm range (40,41). The -OH functional group is an electron donor that helps to bond positively charged dyes.

#### Adsorption studies of Methylene Blue

The  $q_{max}$  value of 212.766 mg/g at 30°C demonstrates the highest adsorption capacity of MB dye ions on GSANC. In the present study, groundnut shell-activated nano carbon (GSANC) treated with KOH demonstrated an adsorption capacity of 212.766 mg/g, notably higher than groundnut shells activated with K<sub>2</sub>CO<sub>3</sub> (210 mg/g). This adsorption capacity favours GSANC, other activated carbons derived from feedstocks impregnated with KOH and other chemicals. Previously reported ACs properties and  $q_{max}$  values for comparison with GSANC are listed in (Table 7).

**Table 7.**  $q_{max}$  of MB values of the different activated carbons from various precursors and their properties.

S.No.	Precursor/Biomass	Activating agent	Qmax (mg/g)	Reference
1	Groundnut shell	KOH	212.766	<b>This study</b>
2	Sugarcane bagasse waste	KOH	136.5	(43)
3	Dragon fruit peels	KOH	195.2	(44)
4	Bamboo chip	KOH	305.3	(17)
5	Sorghum-Waste	KOH	98.1	(16)
6	Cotton cake	H <sub>3</sub> PO <sub>4</sub>	333.33	(45)
7	Date pits	FeCl <sub>3</sub>	259.25	(46)
8	Groundnut shell	K <sub>2</sub> CO <sub>3</sub>	210	(47)

#### Mechanism of MB adsorption on GSANC

GSANC has an excellent porous structure, surface area, and various surface functional groups, enabling efficient MB dye ion removal. Its microporous and mesoporous structure aids dye ion diffusion. The MB ion removal is governed by  $\pi$ - $\pi$  stacking, electrostatic interactions, and hydrogen bonding (Fig. 21.). The negatively charged GSANC enhances removal through hydrogen bonding and electrostatic interactions with the cationic dye. Additionally,  $\pi$ - $\pi$

stacking occurs between the aromatic rings of the MB dye and the hexagonal structure of GSANC, which contains electron-donating groups like -OH (42).

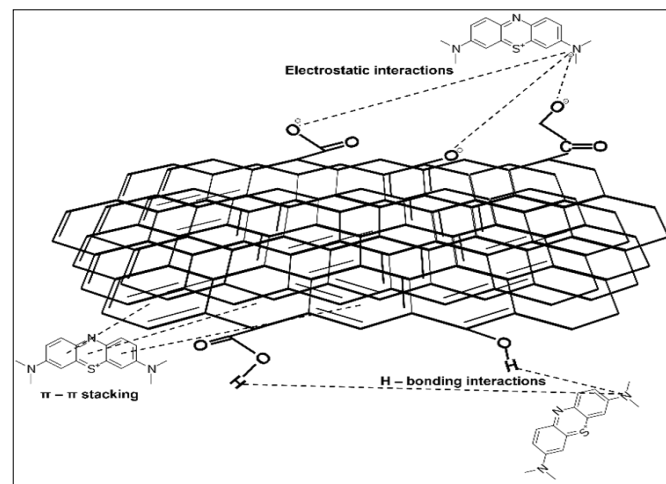


**Fig. 21.** Schematic illustration of MB dye molecules' interaction with GSANC by electrostatic interactions,  $\pi$ - $\pi$  stacking, and H-bonding interactions.

#### Conclusion

In conclusion, the activated carbon derived from groundnut shells (GSANC) demonstrated excellent adsorption capabilities for methylene blue, primarily attributed to its high surface area, well-developed porosity, and favourable surface chemistry. The materials' microporous and mesoporous structure, confirmed through various characterization techniques such as BET, FE-SEM, and XRD, enhanced their adsorption performance. Functional group analysis through FT-IR, thermal stability from TGA, and particle size analysis further highlighted its suitability as an efficient adsorbent. The combination of these properties underscores GSANC's potential as a highly effective material for dye removal. GSANC is also suitable for adsorbing pharmaceutical compounds, heavy metals, pesticides, and phenolic compounds.

#### Acknowledgements

The authors acknowledge the Department of Environmental Sciences, TNAU, Coimbatore, for funding this research under the Sanitation First India Limited Scheme (Scheme number: F37AMZ).

#### Authors' contributions

MTGR conducted experimental studies on activated carbon for methylene blue (MB) adsorption and drafted the

manuscript. PCP conceived the study and contributed to its design and methodology. JP participated in kinetic and mathematical modelling. JSSD interpreted the results, and VP gave input for characterizing the adsorbent materials. RK and PMS supervised the overall direction and coordination of the research. All authors read and approved the final manuscript.

## Compliance with ethical standards

**Conflict of interest:** Authors do not have any conflict of interests to declare.

**Ethical issues:** None

## References

1. Benkhaya S, M'rabet S, Lgaz H, El Bachiri A, El Harfi A. Dyes: classification, pollution, and environmental effects. dans: dye biodegradation, mechanisms and techniques: recent advances. Springer; 2022. [https://doi.org/10.1007/978-981-16-5932-4\\_1](https://doi.org/10.1007/978-981-16-5932-4_1)
2. Hashemi SH, Kaykhahi M. Azo dyes: Sources, occurrence, toxicity, sampling, analysis, and their removal methods. dans: emerging freshwater pollutants. Elsevier; 2022. <https://doi.org/10.1016/B978-0-12-822850-0.00013-2>
3. Salimi A, Roosta A. Experimental solubility and thermodynamic aspects of methylene blue in different solvents. *Thermochim Acta*. 2019;675:134-9.
4. Eldeeb TM, Aigbe UO, Ukhurebor KE, Onyancha RB, El-Nemr MA, Hassaan MA, et al. Adsorption of methylene blue (MB) dye on ozone, purified and sonicated sawdust biochars. *Biomass Convers Biorefin*. 2024;14(8):9361-83. <https://doi.org/10.1007/s13399-022-03015-w>
5. Sen TK. Adsorptive Removal of dye (methylene blue) organic pollutant from water by pine tree leaf biomass adsorbent. *Processes*. 2023;11(7):1877. <https://doi.org/10.3390/pr11071877>
6. Supong A, Bhomick PC, Baruah M, Pongener C, Sinha UB, Sinha D. Adsorptive removal of Bisphenol A by biomass activated carbon and insights into the adsorption mechanism through density functional theory calculations. *Sustain Chem Pharm*. 2019;13:100159. <https://doi.org/10.1016/j.scp.2019.100159>
7. Tsade Kara H, Anshebo ST, Sabir FK, Adam Workineh G, Delele MA, directeur. Removal of methylene blue dye from wastewater using periodiated modified nanocellulose. *International Journal of Chemical Engineering*. 2021;2021(1):1-16. <https://doi.org/10.1155/2021/9965452>
8. Sawalha H, Bader A, Sarsour J, Al-Jabari M, Rene ER. Removal of dye (methylene blue) from wastewater using bio-char derived from agricultural residues in Palestine: performance and isotherm analysis. *Processes*. 2022;10(10). <https://doi.org/10.3390/pr10102039>
9. Zhou Y, Zhang L, Cheng Z. Removal of organic pollutants from aqueous solution using agricultural wastes: A review. *J Mol Liq*. 2015;212:739-62. <https://doi.org/10.1016/j.molliq.2015.10.023>
10. AL-Othman ZA, Ali R, Naushad Mu. Hexavalent chromium removal from aqueous medium by activated carbon prepared from peanut shell: Adsorption kinetics, equilibrium and thermodynamic studies. *Chemical Engineering Journal*. 2012;184:238-47. <https://doi.org/10.1016/j.cej.2012.01.048>
11. Shan R, Shi Y, Gu J, Wang Y, Yuan H. Single and competitive adsorption affinity of heavy metals toward peanut shell-derived biochar and its mechanisms in aqueous systems. *Chin J Chem Eng*. 2020;28(5):1375-83. <https://doi.org/10.1016/j.cjche.2020.02.012>
12. Nam H, Wang S, Jeong HR. TMA and H<sub>2</sub>S gas removals using metal loaded on rice husk activated carbon for indoor air purification. *Fuel*. 2018;213:186-94. <https://doi.org/10.1016/j.fuel.2017.10.089>
13. Xu Z, Chen J, Zhang X, Song Q, Wu J, Ding L, et al. Template-free preparation of nitrogen-doped activated carbon with porous architecture for high-performance supercapacitors. *Microporous and Mesoporous Materials*. Elsevier; 2019;276:280-91. <https://doi.org/10.1016/j.micromeso.2018.09.023>
14. Wang B, Qiu J, Feng H, Sakai E, Komiyama T. KOH-activated nitrogen doped porous carbon nanowires with superior performance in supercapacitors. *Electrochim Acta*. 2016;190:229-39. <https://doi.org/10.1016/j.electacta.2016.01.038>
15. Sing KSW. Reporting physisorption data for gas/solid systems with special reference to the determination of surface area and porosity (Recommendations 1984). *Pure and Applied Chemistry*. 1985;57(4):603-19. <https://doi.org/10.1351/pac198557040603>
16. Hou J, Liu Y, Wen S, Li W, Liao R, Wang L. Sorghum-waste-derived high-surface area koh-activated porous carbon for highly efficient methylene blue and Pb(II) Removal. *ACS Omega*. 2020;5(23):13548-56. <https://doi.org/10.1021/acsomega.9b04452>
17. Jawad AH, Abdulhameed AS. Statistical modeling of methylene blue dye adsorption by high surface area mesoporous activated carbon from bamboo chip using KOH-assisted thermal activation. *Energy Ecol Environ*. 2020;5(6):456-69. <https://doi.org/10.1007/s40974-020-00177-z>
18. Inyang M, Gao B, Yao Y, Xue Y, Zimmerman AR, Pullammanappallil P, et al. Removal of heavy metals from aqueous solution by biochars derived from anaerobically digested biomass. *Bioresour Technol*. 2012;110:50-6. <https://doi.org/10.1016/j.biortech.2012.01.072>
19. Li M, Li W, Liu S. Hydrothermal synthesis, characterization, and KOH activation of carbon spheres from glucose. *Carbohydr Res*. 2011;346(8):999-1004.
20. International Biochar Initiative. [En ligne]. 2015. Specification standards: standardized product definition and product testing guidelines for biochar that is used in soil (aka IBI Biochar Standards) [cité le 27 sept 2024].
21. EBC I. Www. European-biochar. Org/en/home ibi biochar stand first publ may [en ligne]. 2012. Comparison of european biochar certificate version 4. 8 and ibi biochar standards version 2.0 european biochar certificate first publication march 2012b [cité le 27 Sept 2024].
22. Lagergren S. About the theory of so-called adsorption of soluble substances. *Kungliga Svenska Vetenskapsakademiens Handlingar*; 1898 [cité le 27 Sept 2024].
23. Ho YS, McKay G. Pseudo-second order model for sorption processes. *Process Biochemistry*. Elsevier; 1999;34(5):451-65. [https://doi.org/10.1016/S0032-9592\(98\)00112-5](https://doi.org/10.1016/S0032-9592(98)00112-5)
24. Senthilkumar S, Varadarajan PR, Porkodi K, Subbhuraam CV. Adsorption of methylene blue onto jute fiber carbon: kinetics and equilibrium studies. *J Colloid Interface Sci*. Elsevier; 2005;284(1):78-82. <https://doi.org/10.1016/j.jcis.2004.09.027>
25. Langmuir I. The constitution and fundamental properties of solids and liquids. Part i. Solids. *J Am Chem Soc*. 1916;38(11):2221-95. <https://doi.org/10.1021/ja02268a002>
26. Bulut Y, Aydin H. A kinetics and thermodynamics study of methylene blue adsorption on wheat shells. *Desalination*. Elsevier; 2006;194(1-3):259-67. <https://doi.org/10.1016/j.desal.2005.10.032>
27. Temkin MJ, Pyzhev V. Recent modifications to Langmuir isotherms. *Acta Physico-Chimica Sinica*; 1940.

28. Weber G, van't Hoff revisited: enthalpy of association of protein subunits. *J Phys Chem.* 1995;99(3):1052-9. <https://doi.org/10.1021/j100003a031>
29. Kumari G, Soni B, Karmee SK. Synthesis of activated carbon from groundnut shell via chemical activation. *Journal of the Institution of Engineers (India): Series E.* 2022;103(1):15-22. <https://doi.org/10.1007/s40034-020-00176-z>
30. Liu Z, Sun Y, Xu X, Qu J, Qu B. Adsorption of Hg(II) in an aqueous solution by activated carbon prepared from rice husk using KOH activation. *ACS Omega.* ACS Publications; 2020;5(45):29231-42. <https://doi.org/10.1021/acsomega.0c03992>
31. Zhao B, O'Connor D, Zhang J, Peng T, Shen Z, Tsang DCW, et al. Effect of pyrolysis temperature, heating rate, and residence time on rapeseed stem derived biochar. *J Clean Prod.* Elsevier; 2018;174:977-87. <https://doi.org/10.1016/j.jclepro.2017.11.013>
32. Alam N, Mokaya R. Evolution of optimal porosity for improved hydrogen storage in templated zeolite-like carbons. *Energy Environ Sci.* The Royal Society of Chemistry; 2010;3(11):1773-81. <https://doi.org/10.1039/C0EE00154F>
33. Faraji M, Saidi M. Experimental and simulation study of peanut shell-derived activated carbon and syngas production via integrated pyrolysis-gasification technique. *Process Safety and Environmental Protection.* 2023;171:874-87. <https://doi.org/10.1016/j.psep.2023.01.052>
34. Mani D, Elango D, Priyadharsan A, Al-Humaid LA, Al-Dahmash ND, Ragupathy S, et al. Groundnut shell chemically treated with KOH to prepare inexpensive activated carbon: Methylene blue adsorption and equilibrium isotherm studies. *Environ Res.* 2023;231:116026. <https://doi.org/10.1016/j.envres.2023.116026>
35. Taleb R, Qasim B. Potassium hydroxide activated peanut shell as an effective adsorbent for the removal of zinc, lead and cadmium from wastewater. *Journal of Ecological Engineering.* 2023;24(1):66-78. <https://doi.org/10.12911/22998993/156006>
36. Cao Y, Wang K, Wang X, Gu Z, Fan Q, Gibbons W, et al. Hierarchical porous activated carbon for supercapacitor derived from corn stalk core by potassium hydroxide activation. *Electrochim Acta.* 2016;212:839-47. <https://doi.org/10.1016/j.electacta.2016.07.069>
37. A Ariharan, B Viswanathan. Porous activated carbon material derived from sustainable bio-resource of peanut shell for H<sub>2</sub> and CO<sub>2</sub> storage applications. *Indian Journal of Chemical Technology.* 2018;25(2):140-9.
38. Lv P, Almeida G, Perré P. TGA-FTIR Analysis of torrefaction of lignocellulosic components (cellulose, xylan, lignin) in isothermal conditions over a wide range of time durations. *Biore-sources.* 2015;10(3):4239-51. <https://doi.org/10.15376/biores.10.3.4239-4251>
39. Pandey MP, Kim CS. Lignin depolymerization and conversion: A review of thermochemical methods. *Chem Eng Technol.* 2011;34(1):29-41. <https://doi.org/10.1002/ceat.201000270>
40. Lian F, Xing B, Zhu L. Comparative study on composition, structure, and adsorption behavior of activated carbons derived from different synthetic waste polymers. *J Colloid Interface Sci.* 2011;360(2):725-30. <https://doi.org/10.1016/j.jcis.2011.04.103>
41. Xing S, Hu C, Qu J, He H, Yang M. Characterization and reactivity of mnx supported on mesoporous zirconia for herbicide 2,4-d mineralization with ozone. *Environ Sci Technol.* 2008;42(9):3363-8. <https://doi.org/10.1021/es0718671>
42. Guo S, Zou Z, Chen Y, Long X, Liu M, Li X, et al. Synergistic effect of hydrogen bonding and π-π interaction for enhanced adsorption of rhodamine B from water using corn straw biochar. *Environmental Pollution.* 2023;320:121060. <https://doi.org/10.1016/j.envpol.2023.121060>
43. Jawad AH, Abdulhameed AS, Bahrudin NN, Hum NNMF, Surip SN, Syed-Hassan SSA, et al. Microporous activated carbon developed from KOH activated biomass waste: surface mechanistic study of methylene blue dye adsorption. *Water Science and Technology.* 2021;84(8):1858-72. <https://doi.org/10.2166/wst.2021.355>
44. Jawad AH, Saud Abdulhameed A, Wilson LD, Syed-Hassan SSA, ALOthman ZA, Rizwan Khan M. High surface area and mesoporous activated carbon from KOH-activated dragon fruit peels for methylene blue dye adsorption: optimization and mechanism study. *Chin J Chem Eng.* 2021;32:281-90. <https://doi.org/10.1016/j.cjche.2020.09.070>
45. Ibrahim T. Kinetics of the Adsorption of anionic and cationic dyes in aqueous solution by low-cost activated carbons prepared from sea cake and cotton cake. *American Chemical Science Journal.* 2014;4(1):38-57. <https://doi.org/10.9734/ACSJ/2014/5403>
46. Theydan SK, Ahmed MJ. Adsorption of methylene blue onto biomass-based activated carbon by FeCl<sub>3</sub> activation: Equilibrium, kinetics, and thermodynamic studies. *J Anal Appl Pyrolysis.* 2012;97:116-22. <https://doi.org/10.1016/j.jaap.2012.05.008>
47. Liu Y, Guo Y, Gao W, Wang Z, Ma Y, Wang Z. Simultaneous preparation of silica and activated carbon from rice husk ash. *J Clean Prod.* 2012;32:204-9. <https://doi.org/10.1016/j.jclepro.2012.03.021>